Electronic Supplementary Information

Effect of surface overlayer in enhancing the photoelectrochemical water oxidation of *in-situ* grown one dimensional spinel zinc ferrite nanorods directly onto the substrate

EXPERIMENTAL SECTION

Materials. All of the chemicals used for experiments were of analytical grade. Milli-Q water (18.2 MΩ) was used for solution preparation and synthesis. Anhydrous ferric chloride, sodium nitrate, aluminium nitrate nonahydrate, and hydrochloric acid were purchased from Merck. Zinc nitrate hexahydrate, and sodium hydroxide were purchased from Sigma-Aldrich. Fluorine doped tin oxide (FTO) coated glass slide (surface resistivity ~7 Ω/sq) were purchase from Sigma-Aldrich.

***Insitu* growth of $ZnFe_2O_4$ by β - FeOOH route:**

The $ZnFe_2O_4$ photoanode was fabricated on the FTO substrate by modification of a previously reported two-step solution method.[S1, S2] First, to a 100 mL teflon-lined stainless steel autoclave containing 30 mL of an aqueous solution of 0.15 M ferric chloride ($FeCl_3$, 97%) and 1 M sodium nitrate ($NaNO_3$, 99%) and 158 µL hydrochloric acid (HCl, wt 36%), four pieces of cleaned FTO substrate were put with the conducting layer facing upward. The autoclave was heated at 95 °C for 4 hours. This results in the formation of a uniform layer of yellow β-FeOOH nanorods over the FTO substrate. The FeOOH-coated substrate was then washed with deionized water and ethanol to remove any residual salt. The as prepared β-FeOOH film were dipped in to a solution containing 1M $Zn(NO_3)_2.6H_2O$ for 30 minutes. The wet electrode was transferred to a furnace which was already heated to 550 °C and annealed for 2 hours. During the annealing process, the β-FeOOH nanorods turned into $ZnFe_2O_4$ nanorods wrapped with an excess ZnO layer. This unwanted ZnO skin was removed by soaking in a 1 M NaOH solution for 12 h with stirring. To reduce the surface defect sites, the $ZnFe_2O_4$ nanorods were treated again at 550°C for 1 hour or 800°C for 10 minutes.

Synthesis of Al_2O_3 coated $ZnFe_2O_4$ nanorods

The as-prepared $ZnFe_2O_4$-800 films were coated with Al_2O_3 overlayers by chemical bath deposition(CBD) method.[S3] In this method, the $ZnFe_2O_4$ films were dipped in to a 200 mL solution containing 1 gm $Al(NO_3)_3.9H_2O$ and 0.8 gm urea for 90°C for 60 minutes. After that the films were dried and annealed at 550°C for 2 hours in a muffle furnace. The as prepared film was named as $ZnFe_2O_4$-Al_2O_3.

It is found that reaction time is very crucial for 1-D growth of β-FeOOH nanostructures. With the increase in the reaction time, urchin like structures grows over the nanorods as shown in Figure S1 (b & c). Hence, the reaction time was optimized to 4 hours for uniform and 1-D growth of β-FeOOH nanorods (Figure S1a). All the annealing temperatures were chosen such that it does not affect the conductivity of the FTO substrate. The post annealing treatment of $ZnFe_2O_4$, after etching ZnO layer, was done to reduce the surface defects such as dangling bonds or lattice disorder which could have facilitated nonradiative recombination.[S2] The cross-sectional FESEM image of β-FeOOH confirms the formation of nanorods, whereas the cross-sectional FESEM images $ZnFe_2O_4$-800 and $ZnFe_2O_4$-Al_2O_3 shows some deformation of these nanorods due to high temperature annealing (Figure S1 (d-f).

Material Characterization. The powder X-ray diffraction measurements were performed using Rigaku TTRAX III X-ray diffractometer where Copper Kα (λ = 1.54 Å) was used as the source with 18kW power. The XRD patterns for the 2θ range of 20°−70° was recorded at the scan rate 0.3°/s. For the measurement of UV−visible absorption spectra, a JASCO (Model V-650) spectrophotometer was used. The Fourier transform infrared (FT-IR) spectra was recorded using PerkinElmer Spectrum Two instrument in KBr pellets by scratching the as prepared films. Raman spectra analysis was done using Laser Micro Raman System (Horiba Jobin Vyon, Model LabRam HR) with 488 nm laser excitation. To know the surface morphology, the FESEM of all of the samples was investigated on a Zeiss (model- Gemini and Sigma) instrument operated at 5 kV. FETEM measurements of the samples were carried out in a JEOL (JEM-2100F) microscope with an operating voltage of 200 kV. X-ray photoelectron spectroscopy (XPS) were carried out using an ESCALAB Xi+ (Made: Thermo Fisher Scientific Pvt. Ltd., UK) photoelectron spectrometer with a monochromatized Al-K_α ($h\nu$ = 1486.6 eV) X-ray source of. In this analysis, all the peaks were referenced with respect to C 1s spectrum (284.77 eV) to compensate the surface charging effect and by the help of XPSPEAK 4.1 software, all XPS core level spectral data were analyzed.

Incident photon-to-current conversion efficiency (IPCE) of the photoanodes were measured in a Newport Oriel IQE-200 instrument with a 250 W quartz tungsten halogen (QTH) lamp as the light source.

Photoelectrochemical measurements. The photoelectrochemical measurements of the samples were performed with an electrochemical analyzer (model-CHI1120B) in a three-electrode system. 1M NaOH solution was used as electrolyte during measurements. As fabricated samples were used as working electrodes, Ag/AgCl(aqueous) electrode was used as reference and a Pt wire was used as counter electrode. All the potential applied were converted into reversible hydrogen electrode (RHE) potential by following formula:

$$\mathbf{E_{RHE} = E_{Ag/AgCl} + 0.059pH + E^{o}_{Ag/AgCl}} \quad (01)$$

where E_{RHE} is the converted potential *vs.* RHE, $E_{Ag/AgCl}$ is the experimentally measured potential *vs.* Ag/AgCl, $E^{o}_{Ag/AgCl}$ is the standard potential of Ag/AgCl reference electrode against the RHE (0.1976 V) and pH is the pH of the electrolyte. The light source was provided by a 300 W halogen lamp, and the light intensity was adjusted to 100 mW/cm^2. The electrochemical impedance spectra (EIS) were measured using an electrochemical work station (Model CHI680E, Inc., Austin, TX) in 1 M NaOH aqueous solution in a frequency range of 10,000 Hz to 0.1 Hz with an amplitude of 10 mV under light illumination. Mott–Schottky curves were obtained in a DC potential range from -0.4 to 0.6 V vs. Ag/AgCl with a frequency of 1000 Hz under dark conditions. The flat band (E_{FB}) and carrier density (N_D) of bare $ZnFe_2O_4$ and Al_2O_3 coated $ZnFe_2O_4$ were calculated from the following formula:

$$\frac{1}{C^2} = \frac{1}{N_D e \varepsilon \varepsilon_0}[E - E_{FB} - \frac{kT}{e}] \quad (02)$$

where C is the capacitance of the semiconductor, N_D is the electron carrier density of semiconductor, e is the fundamental charge constant, ε_0 is the permittivity of the vacuum, ε is the relative permittivity of the semiconductor, E is the applied potential, k is the Boltzmann constant, and T is the temperature.

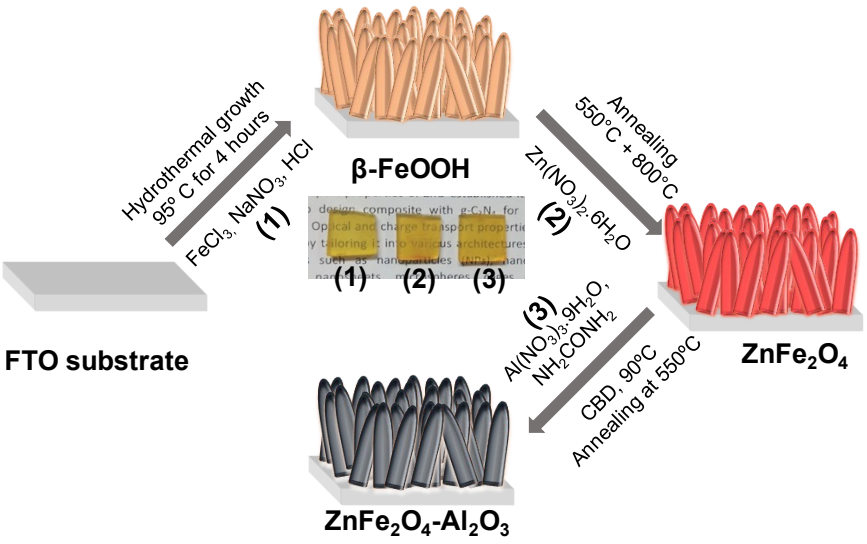

Scheme 1. Step-by-step fabrication of $ZnFe_2O_4$-Al_2O_3 photoanode (1) Fabrication of β-FeOOH nanorods over FTO substrate, (2) conversion of β-FeOOH to $ZnFe_2O_4$ by wet dipping of Zn precursor followed by annealing[S2] and (3) deposition of Al_2O_3 over $ZnFe_2O_4$ by chemical bath deposition (CBD) method.

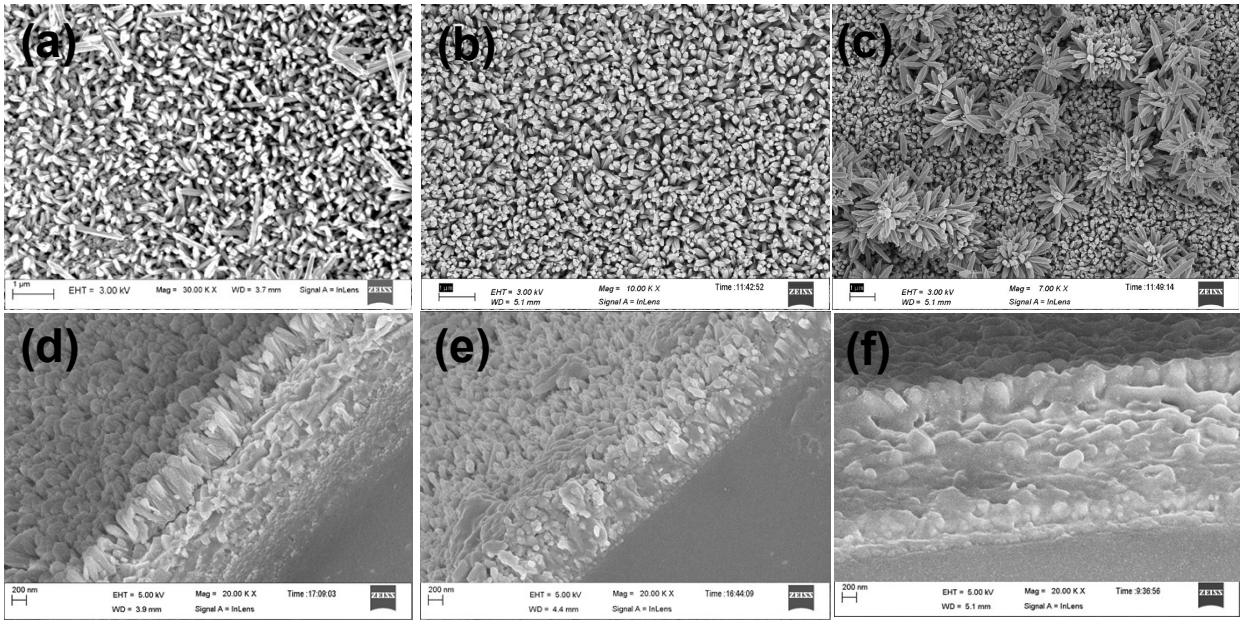

Figure S1. FESEM images showing β-FeOOH nanorods(a), $ZnFe_2O_4$ prepared with different growth time of β-FeOOH nanorods- 4 hours (b) and 6 hours (c), cross-sectional view of β-FeOOH (d), $ZnFe_2O_4$-800 (e) and $ZnFe_2O_4$-Al_2O_3 (f).

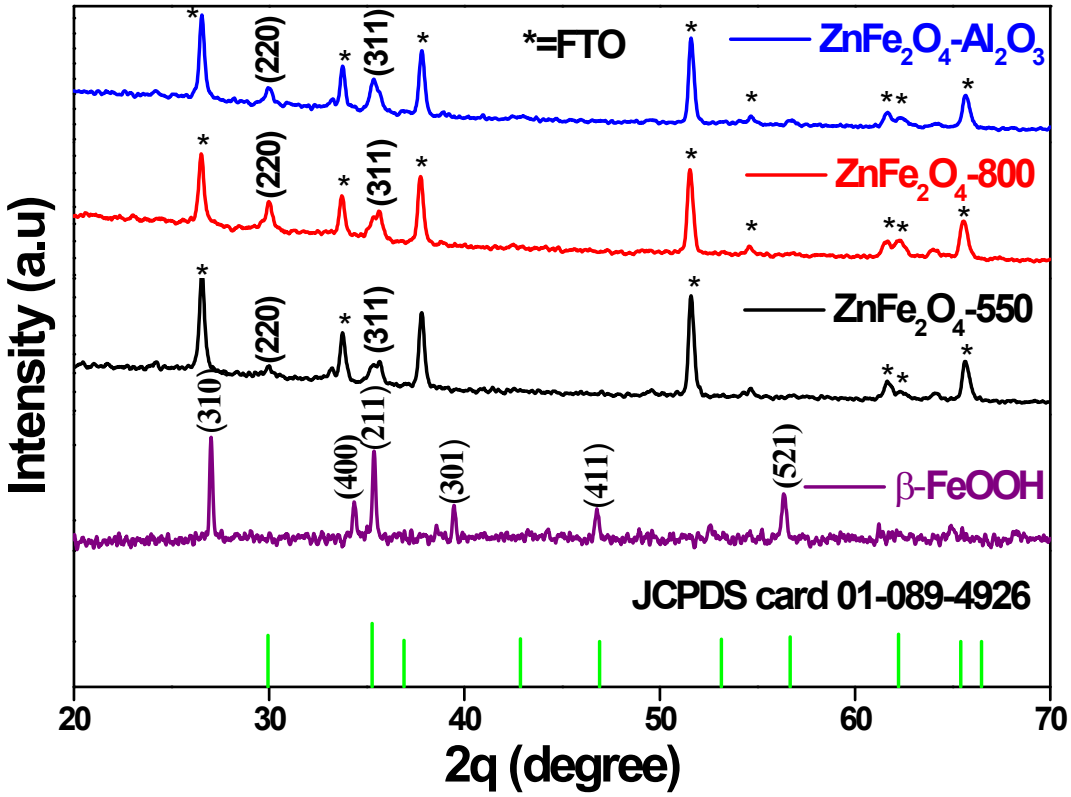

Figure S2. Powder XRD of β-FeOOH, $ZnFe_2O_4$-550, $ZnFe_2O_4$-800 and $ZnFe_2O_4$-Al_2O_3.

The powder XRD of β-FeOOH was well matched with JCPDS card 75-1549. The peaks at 2θ = 30° represent the (220) crystal planes and 2θ=35.2° represent the (311) crystal planes of the cubic spinel $ZnFe_2O_4$ (The green vertical lines represent peaks of cubic spinel $ZnFe_2O_4$, JCPDS card 01-089-4926). There were no impurities of ZnO or Fe_2O_3 present in the XRD pattern of $ZnFe_2O_4$. The weak XRD peaks of $ZnFe_2O_4$ became sharp with further temperature treatment at 800°C. As the films were directly grown over FTO substrate, the peaks of SnO_2 were clearly visible.

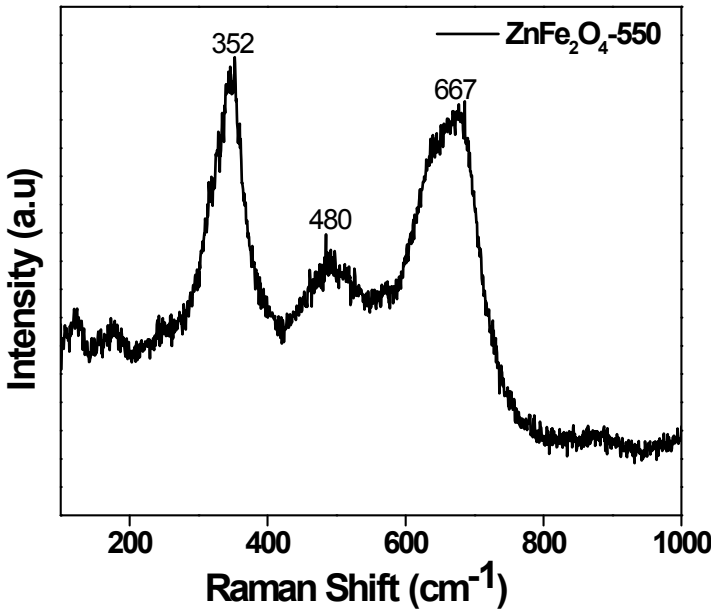

Figure S3. Raman spectra of $ZnFe_2O_4$-800.

$ZnFe_2O_4$ has a spinel structure with space group *Fd3m*. Out of five Raman modes three were observed at 352 cm^{-1}, 480 cm^{-1} and 667 cm^{-1}. The motion of oxygen in tetrahedral AO_4 groups happens at modes above 600 cm^{-1}. These modes can be assigned to A_{1g} symmetry and the other low frequency modes to both E_g and F_{2g} which were the characteristics of the octahedral sites (BO_6).[S4,S5]

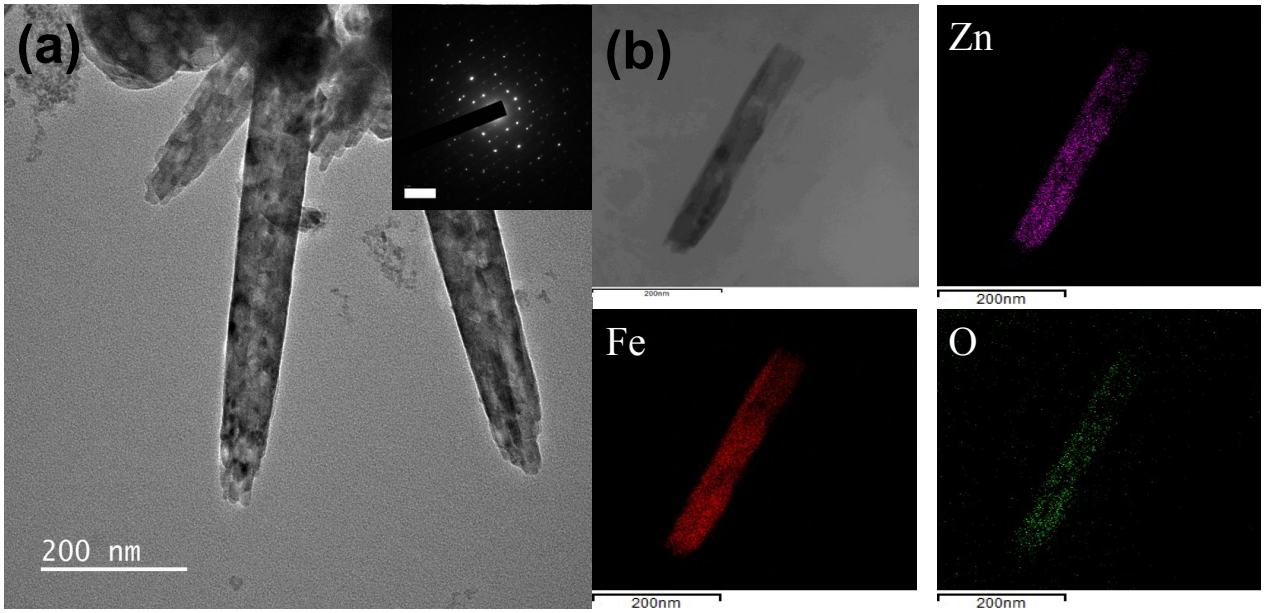

Figure S4. (a)TEM image of $ZnFe_2O_4$-800 and (b) elemental mapping of $ZnFe_2O_4$-800. Inset of (a) showing the SAED pattern of $ZnFe_2O_4$-800. The uniform distribution of all the elements and SAED pattern showing single crystalline phase confirmed the formation of $ZnFe_2O_4$-800.

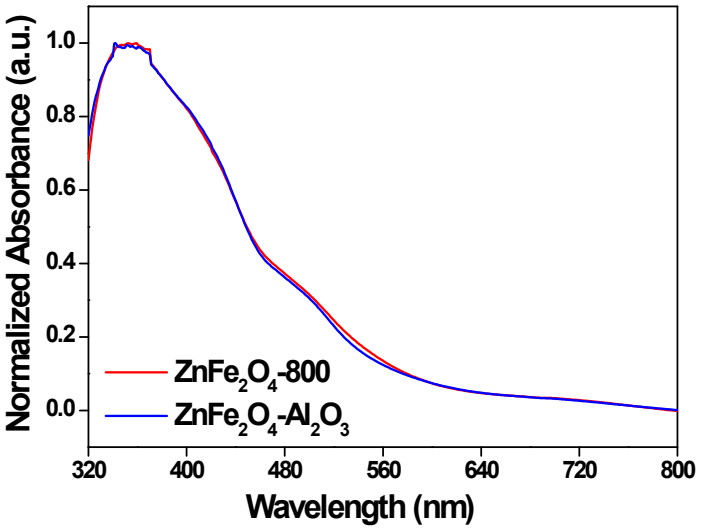

Figure S5. UV-visible spectrum of $ZnFe_2O_4$-800 and $ZnFe_2O_4$-Al_2O_3

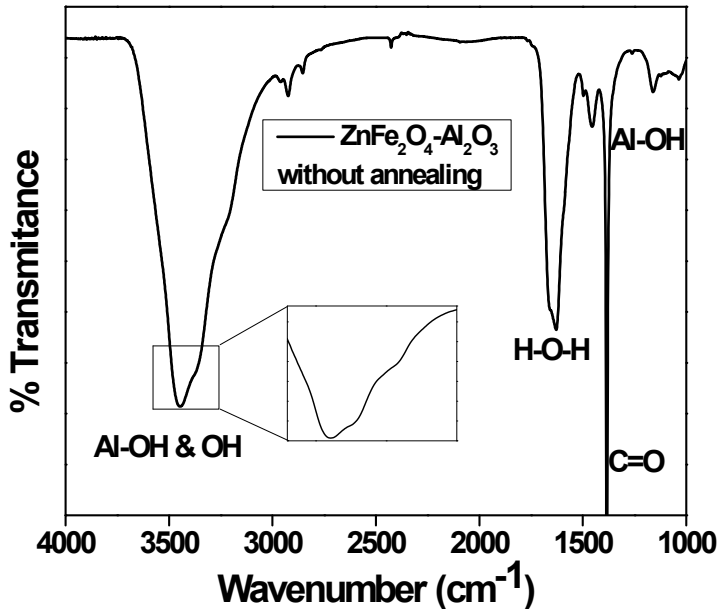

Figure S6. FT-IR spectrum of $ZnFe_2O_4$ treated with CBD process without annealing.

The wavenumber of 1040 cm^{-1} could be assigned to Al-OH bending. The peaks at 3450, 3367 cm^{-1} might be attributed to Al-OH stretching. The 1375 cm^{-1} corresponding to C=O was identified to the urea used in the CBD bath, which will be removed during the annealing treatment. The H-O-H bending exhibits the peak of 1623 cm^{-1}, indicating the absorption of water. [S3]

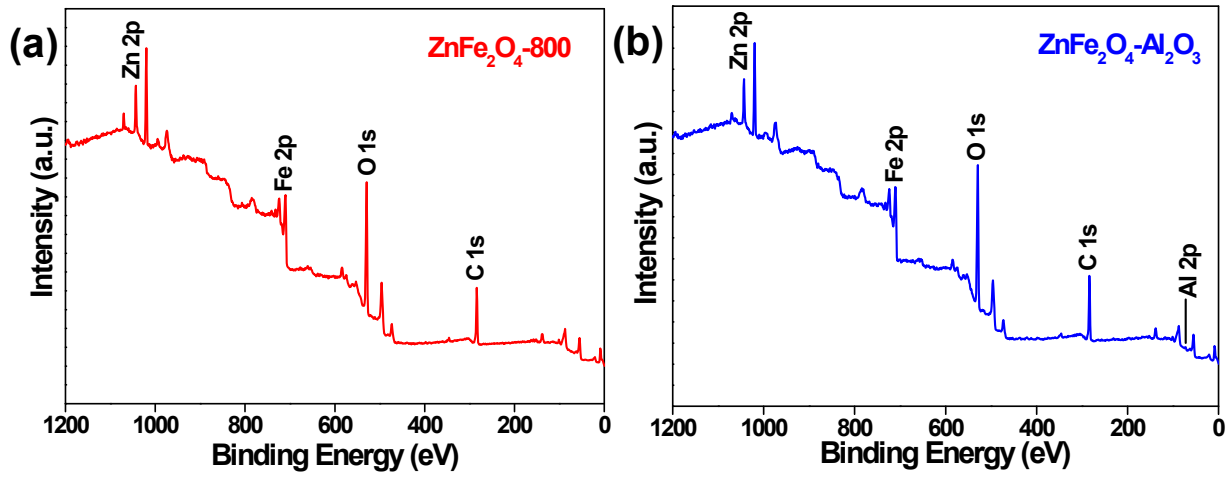

Figure S7. XPS survey spectra of (A) $ZnFe_2O_4$ and (B) $ZnFe_2O_4$-Al_2O_3.

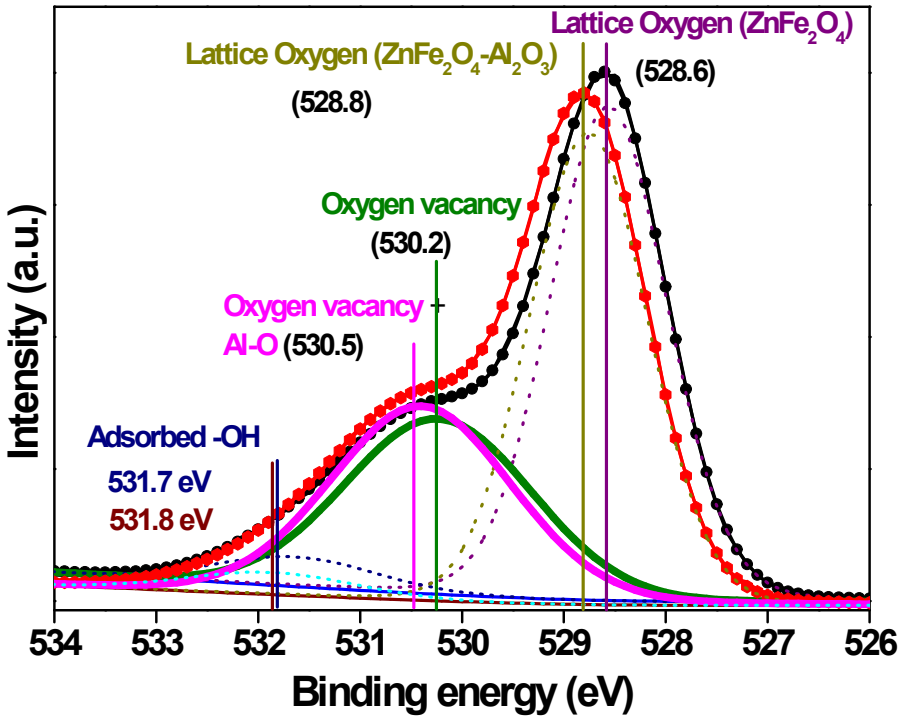

Figure S8. O 1s core level of $ZnFe_2O_4$ (black line) and $ZnFe_2O_4$-Al_2O_3 (red line) where the dotted line in the lower binding energy corresponds to lattice oxygen and the dotted line in the higher binding energy corresponds to adsorbed –OH. In the middle region the peak at 530.2 eV of bare $ZnFe_2O_4$ (olive line) corresponds mainly due to oxygen vacancy and the peak at 530.5 eV of $ZnFe_2O_4$-Al_2O_3 (magenta line) is due to contribution of oxygen vacancy as well as Al-O of alumina, which is confirmed by the shift in this peak towards higher binding energy and increase in peak area as compared to bare $ZnFe_2O_4$.

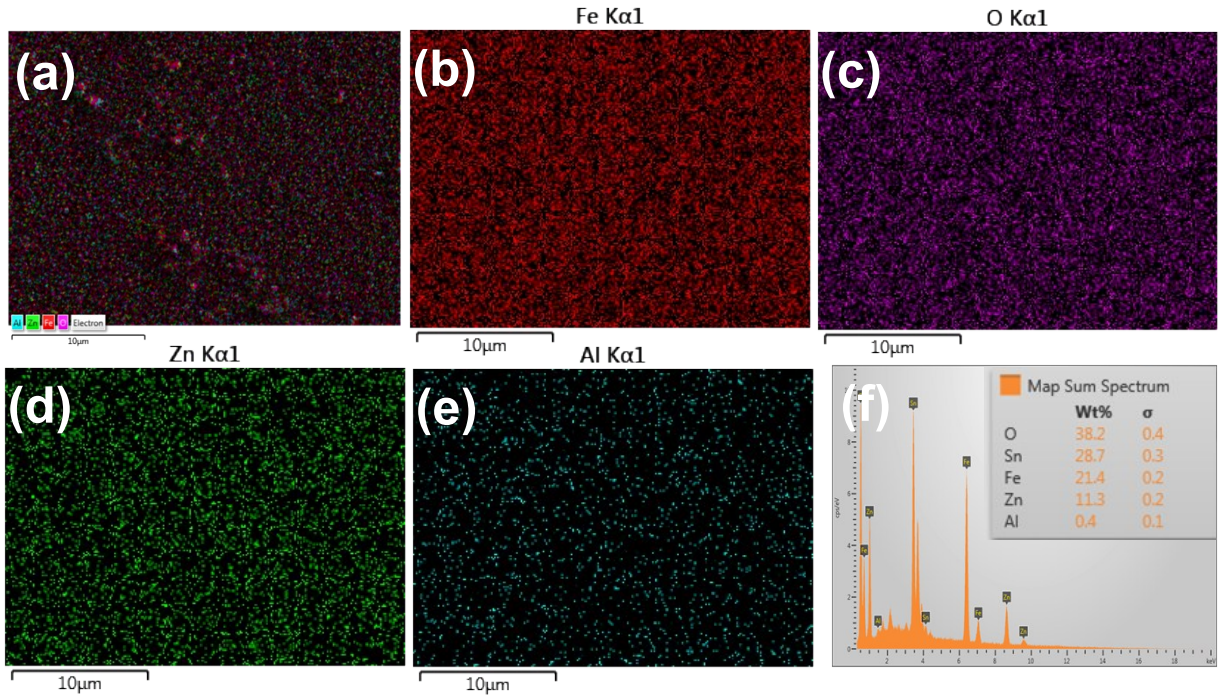

Figure S9. (a) Elemental mapping of $ZnFe_2O_4$–Al_2O_3 showing the uniform distribution of (b) Fe, (c) O, (d) Zn, and (e) Al. (f) FESEM-EDX showing elemental composition.

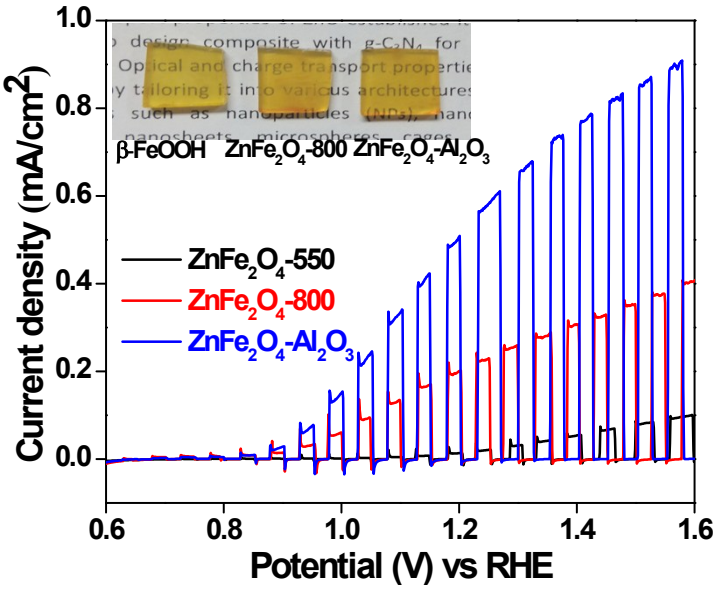

Figure S10. J-V curves of all the photoanodes with chopped light-dark. Inset to the figure showing digital photos of fabricated photoanodes.

The anodic current spikes and cathodic transient peaks of $ZnFe_2O_4$-Al_2O_3 disappeared when the bias was more positive than 1.23 V *vs.* RHE, indicating that accumulation and recombination of holes were prevented by CBD-Al_2O_3. In contrast, the cathodic transient peaks of $ZnFe_2O_4$-550 and $ZnFe_2O_4$-800 were visible after 1.23 V *vs.* RHE. This experimental evidence confirmed that the PEC performance improved with introduction of CBD-Al_2O_3.

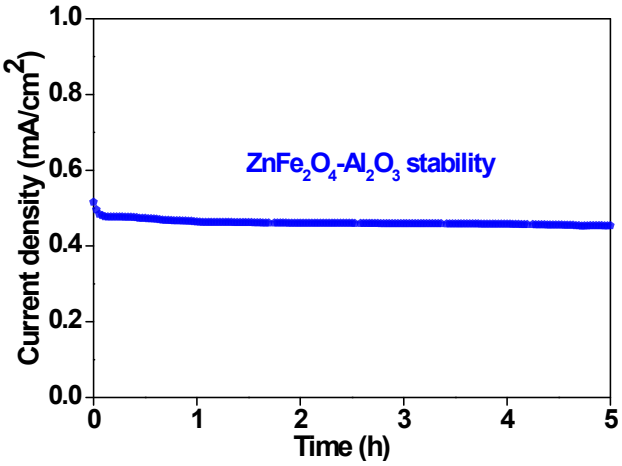

Figure S11. Stability of $ZnFe_2O_4$-Al_2O_3 photoanode under light illumination at 1.23 V *vs.* RHE.

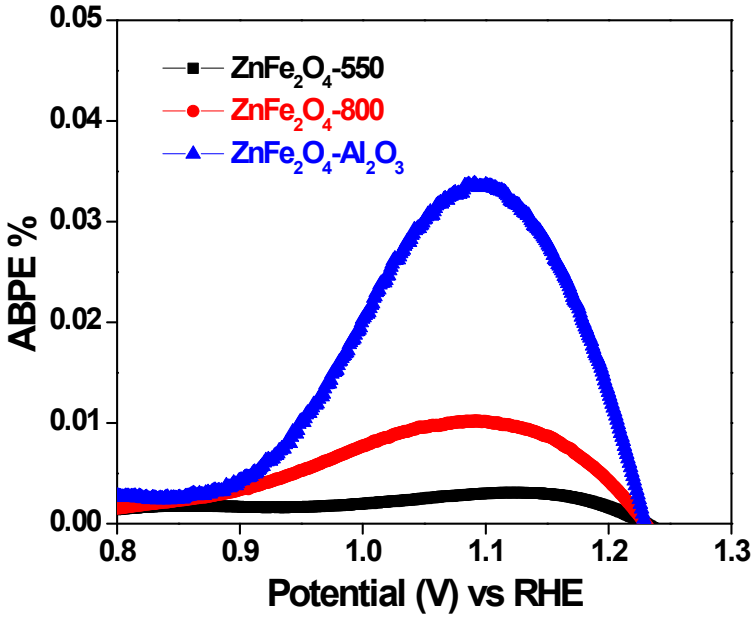

Figure S12. The applied bias photon-to-current efficiencies (ABPE) of all the photoanodes to quantitatively evaluate the PEC water oxidation efficiency. A maximum of 0.034% photoconversion efficiency was achieved for the $ZnFe_2O_4$-Al_2O_3 photoanode at 1.1 V vs. RHE, which was 11 and 3 times higher than that of $ZnFe_2O_4$-550 and $ZnFe_2O_4$-800, respectively.

The applied bias photon-to-current efficiency (ABPE) was calculated using the following equation:

$$ABPE = [\frac{J_{photo}(1.23 - V)}{P}] \quad \text{(S3)}$$

Where V is the voltage that is applied *vs.* RHE to the cell from an external power source and J_{photo} is the photocurrent measured at this voltage and P is the power density of incident light. [S6]

Table S1. Comparison with similar literature reports

Photoanodes	**Fabrication method**	**Photocurrent (1.23 V vs RHE)**	**References**

Hydrogen treated $ZnFe_2O_4$	Solvothermal method	320 µA	S1
HMA treatment of $ZnFe_2O_4$	Solvothermal method	240 µA	S2
Hydrogen treated $ZnFe_2O_4$	Solvothermal method	200 µA	S4
$ZnFe_2O_4$	Aerosol-assisted chemical vapour deposition	350 µA (1.15 V vs. RHE)	S5
macroporous ATO coated $ZnFe_2O_4$	Atomic layer deposition	260 µA	S7
Ti-doped $ZnFe_2O_4$	Spray pyrolysis method	350 µA	S8
$SrTiO_3$:$ZnFe_2O_4$	Pulsed laser deposition	188 µA	S9
$ZnFe_2O_4$	Chemical vapour deposition	85 µA (1.6 vs RHE)	S10
$ZnFe_2O_4$-Al_2O_3	Solvothermal method	**484 µA (0.48 mA)**	This study

References

S1. J. H. Kim, Y. J. Jang, J. H. Kim, J.-W. Jang, S. H. Choi, J. S. Lee, *Nanoscale*, 2015, **7**, 19144.

S2. J. H. Kim, J. H. Kim, J.-W.Jang, J. Y. Kim, S. H. Choi, G. Magesh, J. Lee, J. S. Lee, *Adv. Energy Mater.*, 2015, **5**, 1401933.

S3. Z. Fan, Z. Xu, S. Yan, Z. Zou, *J. Mater. Chem. A*, 2017, **5**, 8402.

S4. N. Guijarro, P. Bornoz, M. Pr´evot, X. Yu, X. Zhu, M. Johnson, X. Jeanbourquin, F. Le Formal and K. Sivula, *Sustainable Energy Fuels*, 2018, **2**, 103.

S5. A. A. Tahir, K. G. U. Wijayantha, *J. Photochem. Photobiol., A*, 2010, **216**, 119.

S6. H. Dotan, N. Mathews, T. Hisatomi, M. Gra¨tzel, A. Rothschild, *J. Phys. Chem. Lett.*, 2014, **5**, 3330.

S7. A. G. Hufnagel, K. Peters, A. Müller, C. Scheu, D. Fattakhova-Rohlfing, T. Bein, *Adv. Funct. Mater.*, 2016, **26**, 4435.

S8. Y. Guo, N. Zhang, X. Wang, Q. Qian, S. Zhang, Z. Li, Z. Zou, *J. Mater. Chem. A*, 2017, **5**, 7571.

S9. S. Cho, J.-W. Jang, L. G. Li, J. Jian, H. Y. Wang, J. L. MacManus-Driscoll, *Chem. Mater.*, 2016, **28**, 3017.

S10. D. Peeters, D. H. Taffa, M. M. Kerrigan, A. Ney, N. Jöns, D. Rogalla, S.Cwik, H.-W. Becker, M. Grafen, A. Ostendorf, C. H. Winter, S. Chakraborty, M. Wark, A. Devi, *ACS Sustainable Chem. Eng.*, 2017, **5**, 2917.